Lightning flashes at electric power system towers identified as Recurrent Lightning Spots observed by ground and space-based systems

S. Ardila, J. Montanyà, J. López, G. Solà and, A. Roncancio

***Abstract*-- This study integrates space-based optical detections with ground-based measurements of lightning flashes on electric power system towers forming Recurrent Lightning Spots (RLS). We found that the lightning-tall tower interaction was related to downward leaders from the thunderstorm charge regions, with no upward flashes recorded. Likewise, cloud-to-ground (CG) strokes in RLSs associated with fast downward leaders exhibit the highest magnitude currents. Our findings suggest that thunderstorms' lower positive charge regions may contribute to increased lightning activity at RLS and revealed a correlation between lightning strokes in RLS with high peak currents and elevated values of integrated optical energy. We identified that the leader's propagation altitude and type and the VHF power emitted by lightning leaders are influential factors in detecting CG strokes from space.**

***Keywords*: RLS, GLM, LMA, tall towers, lightning interaction.**

I. Introduction

Tall structures, such as electric power system towers, are likelier to be struck by lightning than lower surroundings and objects[1]. This increased exposure can lead to interruptions in the electricity supply and negatively impact power quality indices [2]. Research indicates that lightning strikes to power lines are influenced by two main factors: the striking distance and the Ground Flash Density of the area (GFD) [3], [4]. Likewise, studies like [5], [6] have shown that tall structures raise the GFD in the vicinity, and the frequency of upward lightning increases with its height [7]. In temperate zones, due to the frequent occurrence of upward lightning related to tall objects, it is relatively easy to identify structures frequently struck by lightning, as they form areas of high lightning activity, characterized by elevated GFD levels at the structures compared to their surroundings [8]. Conversely, in tropical regions like Colombia, high GFD values are common, making it challenging for a specific tall structure to exhibit a GFD higher than the average for the area [9].

This work was supported by the Electrical Engineering department of the Polytechnic University of Catalonia

B. S. Ardila is with Electrical Engineering department of the Polytechnic University of Catalonia, 08034, Barcelona, Spain (e-mail of corresponding author: brandon.steven.ardila@upc.edu).

J. Montanyà is with Electrical Engineering department of the Polytechnic University of Catalonia, 08034, Barcelona, Spain (e-mail: joan.montanya@upc.edu).

J. A. López is with Electrical Engineering department of the Polytechnic University of Catalonia, 08034, Barcelona, Spain (e-mail: jesus.alberto.lopez@upc.edu).

G. Solà is with Electrical Engineering department of the Polytechnic University of Catalonia, 08034, Barcelona, Spain (e-mail: gloria.sola@upc.edu).

J. A. Roncancio is with Electrical Engineering department of the Polytechnic University of Catalonia, 08034, Barcelona, Spain (e-mail: jose.andres.roncancio@upc.edu).

Paper submitted to the International Conference on Power Systems Transients (IPST2025) in Guadalajara, Mexico, June 8-12, 2025.

Recently, the new concept known as Recurrent Lightning Spot (RLS) was introduced by [10]. This concept helps identify areas where lightning strikes occur recurrently over successive years. Rather than focusing on the total number of lightning strikes in a given location, this methodology emphasizes the periodicity of their occurrence. An RLS is a geographic location where at least one lightning stroke is recorded annually over multiple years. It was found that RLS are not always situated in areas with high GFD values. Instead, they tend to be associated with tall structures, mountain peaks, and steep terrain. Some RLS have also been identified in open sea areas [10]. Research on lightning strikes affecting tall structures has primarily utilized ground-based systems, including mapping/detection networks, meteorological radar, fast cameras, and instrumented towers. These studies have significantly contributed to our understanding of lightning parameterization [11], [12], [13], the statistical analysis of return currents [14], the attachment process [15], the mechanisms triggering upward lightning [16], [17], the thunderstorm characteristics favoring their occurrence[18], [19], and radar characteristics [20], among others. Recently, space-based optical lightning detections using the Geostationary Lightning Mapper – GLM, have been employed to study lightning strikes on electric power systems [21]. While these optical detection instruments are designed for total lightning monitoring, they cannot distinguish between different types of lightning: intra-cloud (IC) or cloud-to-ground (CG), or provide precise location data as ground-based detection systems can. However, they enable the study of the intracloud processes associated with each flash, as well as the detection of continuous currents and energetic transients related to all flashes, along with other properties resulting from optical emissions [21].

Lightning in electric power system towers classified as RLSs has yet to be studied in tropical regions. Research has shown that in temperate regions, a significant percentage of lightning flashes in tall structures are initiated by upward leaders from the structures themselves, primarily due to their height [22], [23], and favored during winter storms, as the thundercloud electrical charge regions are closer to the ground [16]. This phenomenon must also be examined in tropical regions, where lightning-tall tower interaction is expected to obey parameters such as the peak current [24]. Additionally, space-based lightning detection have yet to be utilized to investigate continuous currents and the intra-cloud development of lightning flashes associated with electric power system towers, which ground-based detection systems cannot record. This article aims to characterize the lightning flashes to RLS corresponding to tall structures such as power transmission line towers. To this purpose, Lightning Mapping Array (LMA) data will be used to investigate if flashes to RLS start with a downward leader to ground or involve precedent in-cloud leader development. LMA will provide

information of the polarity of the leaders, their altitudes and range. Moreover, the Geostationary Lightning Mapper (GLM) will provide optical data related to the flashes at the RLS. Optical energy and stroke peak currents will be investigated in the RLS and in non-RLS sites.

II. Data and Methodology

A. VLF/LF LINET network

Cloud-to-ground (CG) stroke data were obtained from the LINET-Colombia network [25]. LINET consists of 21 sensors with baselines ranging from 150 to 250 km. These sensors detect VLF/LF electromagnetic impulses generated by IC and CG lightning strokes, employing the time-of-arrival technique to locate them in both time and space [26], [27]. This network provides the stroke peak current and polarity, which will be used in this study. To prevent misclassification of CG strokes, those with low currents (-6 kA $\leq$ I $\leq$ 8 kA) were excluded because probably are associated with IC events [10], [28].

B. VHF Lightning Mapping Array - LMA

The study of lightning leader propagation related to CG strokes was conducted using the Colombia Lightning Mapping Array (LMA). This network has been operational in Colombia since 2015 [29] and determines the time of arrival (TOA) of VHF (60-66 MHz) radio emissions generated by electrical breakdown processes [30]. By locating each source in space and time, the network enables the mapping of lightning leader propagation [31], [32]. The Colombia-LMA is located in northeastern Colombia in a high lightning activity zone over the Magdalena River and consists of eight stations with baselines ranging from 7 to 25 km[33].

C. Geostationary Lightning Mapper – GLM

Optical lightning emissions from space are detected by the Geostationary Lightning Mapper (GLM). This instrument is on board the GOES-16,17,18 and 19 satellites and provides data of total lightning across the Americas and a large part of the Atlantic and Pacific oceans. GLM cameras observe in a narrowband centered at 777.4 nm producing images every 2 ms, and with a spatial resolution of approximately 8 km at the subsatellite point [34], [35]. The GLM data is categorized into events, groups, and flashes. An event is a single-pixel lightning detection within a 2 ms integration frame. Events in the same integration frame are first clustered into groups, representing contiguous regions illuminated simultaneously [35][36]. These groups are then further clustered into flashes based on their spatio-temporal proximity [35], [37].

D. Methodology

Five hundred forty-nine power transmission line towers (PTTs from now on) with heights between 40 and 134 meters, were located in northeastern Colombia. This area is characterized by high lightning activity, recording up to 60 flashes/km^2/year. PTTs are illustrated in Figure 1.

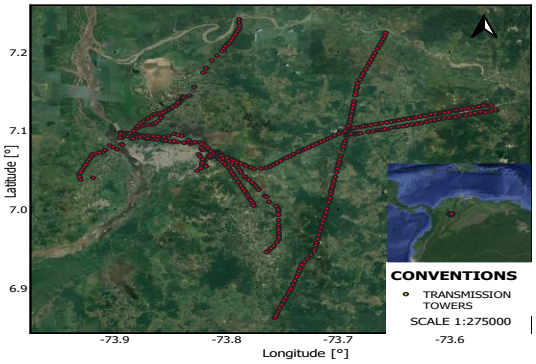

Fig. 1. Location of power transmission line towers in the study zone.

To identify towers that correspond to RLS, the methodology described in [10] is applied. First, lightning recurrence is determined, which requires at least one lightning strike to be recorded at the tower for over ten consecutive years. For this assessment, strokes within a radius of 300 meters of a PTT are considered direct impacts on the tower, due to the average location error of the LINET data [38]. Next, the average ground strike point density (N_{SG}) is calculated up to 1 km from the PTT, as introduced in [10]. For a non-RLS structure, the N_{SG} peaks at the closest distance from the structure and then decays exponentially as one moves away mainly due to the increase of the area with the square of the radius (distance), represented by the orange curve in Figure 2 [10]. When a RLS is present, additional strokes are detected by an LLS close to the location. Since a LLS has some location accuracy (100-200 m for the study zone), the strokes are not just detected at the precise location of the RLS if not scattering around. The above is supported by [25] and [39]. In this work, towers are classified as RLS if the N_{SG} increases exponentially for radial distances less than 100 meters from the PTT, reaching its maximum value in the area surrounding the PTT (100-200 m). Beyond this point, the N_{SG} declines as the distance increases, reaching the typical N_{SG} value for the region at distances greater than 1 km, as illustrated by the blue curve in Figure 2 [10].

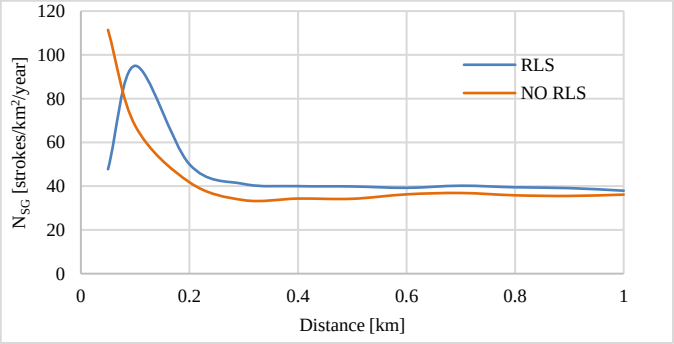

Fig. 2. Average ground strike point density variation as a function of radial distance for a tower classified as RLS and as non-RLS.

Once the RLSs are identified, the CG strokes in these towers are determined using LINET data. Using a clustering algorithm proposed by [40], the sources detected by the LMA during CG strokes in RLSs are grouped into flashes. A LMA-flash is a grouping of sources separated by no more than 150 ms in time [41]. Based on the lightning leaders' initiation and propagation heights, we characterize the LMA-flashes. The flash initiation

height was established using the method proposed in [29]. In this method, the flash initiation point represents the centroid of an area where the standard deviation of the first LMA sources (5 to 10) is less than 500 m. Moreover, lightning leaders' polarity are determined using a time-distance plot of the LMA sources [40]. The LMA-flashes are categorized into two groups to establish patterns: in the first group, flashes show precedent IC leader activity before the CG stroke in a RLS (over 30-50 ms in time). The second group consists of flashes initiating with a downward leader without previous IC leader propagation.

Additionally, coincident GLM detections (events) during the occurrence of strokes in RLSs are clustered into groups and then into flashes. A GLM-flash is a sequential occurrence of groups in less than 330 ms in time and separated by no more than 16.5 km in space [35]. For each GLM-flash, we plot the maximum GLM-optical energy recorded per pixel and the GLM-integrated optical energy, calculated by integrating the energy of all events every 2 ms frame as in [21]. GLM-integrated optical energy will provide the identification of the presence of continuing currents [42]. This method establishes a continuous current component if the GLM-integrated optical energy remains continuously different from zero for at least 8 ms after the CG stroke. Lightning flashes to RLSs with continuous current correspond to our third study group. In addition, the amplitudes of the integrated optical energy pulses at the time of CG strokes will be used to investigate a possible relation between the stroke peak current and optical energy [39]. In this work, we analyzed 50 LMA-flashes and 92 CG strokes to power transmission line towers categorized as RLSs.

III. Results

A. Recurrent Lightning Spots

Figure 3 shows the RLSs associated with power transmission line towers. Many of these towers are located in or near the urban area of Barrancabermeja. However, some towers are situated away from this perimeter. The resulted RLSs are positioned at elevations up to 50 meters above sea level, with slight terrain elevations reaching 200 masl.

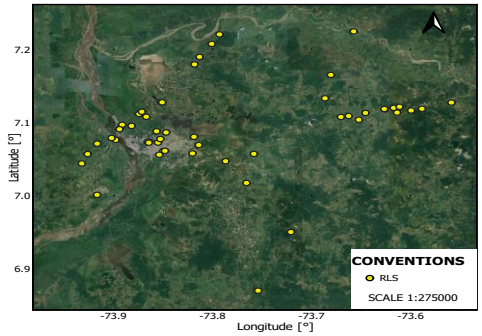

Fig. 3. RLS location in the study zone.

B. IC Activity precedent to CG strokes in RLS

Once the RLS are identified, we first analyze the percentage of flashes at RLS with preceding in-cloud leader activity before the CG strokes to the RLS. The analysis results that among the sample of LMA-flashes in RLSs, 46% exhibit IC development before striking the RLS. As a case of this group of flashes is depicted in Figure 4 and summarized. Panel A in Figure 4 shows the altitude versus time of the LMA sources mapped during a LMA-flash in a RLS. This data is superimposed in time with the CG detections (× symbol) labeled by their peak current. According to the plot, the flash starts around 6 km altitude (black point) with an upward negative leader propagating during 50 ms reaching up to 13 km, while other upward negative leader is mapped exhibiting a broad horizontal propagation for approximately 400 ms at 6-7 km altitude. At the end of this phase, a downward negative leader propagates for about 10 ms, and two CG strokes of -6.6 kA and -77.2 kA are recorded, with the latter located on the RLS. After, another fast downward negative leader is mapped, and a final -14.4 kA CG stroke is registered. According to panel B, GLM provided detections during the flash initiation by an in-cloud upward propagating negative leader, with a maximum of 92.87 fJ. In contrast, no GLM detections were provided during the time of in-cloud negative leader propagation probably due to their lower altitude in the cloud compared with the propagation at the initiation. The integrated optical energy exhibits pulses starting at 30.15 s, reaching maximum values of 213.2 fJ, 744.9 fJ, and 52.86 fJ, respectively. These pulses are associated with CG strokes reported by LINET. The highest value of integrated energy occurs precisely at the moment of the stroke at the RLS, corresponding to the stroke with the maximum current value.

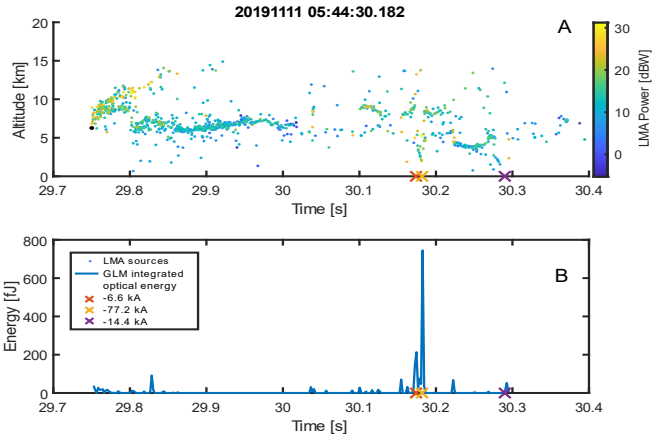

Fig. 4. A) LMA detections altitude vs. time (color-coded by power); B) GLM-integrated optical energy for a flash in a RLS on 11 November 2019 at 05:44:30.182 UTC. Markers (×) indicate the CG strokes.

Figure 5 presents a top view of the GLM-flash. Pixels are characterized according to the maximum GLM optical energy of the events recorded in each pixel. Additionally, the sources mapped by the LMA are shown and color-coded based on the power emitted. The figure also includes CG strokes and the RLS location. According to the figure, the flash exhibited an extension of 24.44 km in latitude and 10.14 km in longitude, with LMA sources emitting VHF power levels up to 31.2 dBW. Moreover, the GLM recorded events with optical energies reaching 159.40 fJ. Notably, GLM events with moderate to high optical energy (greater than 100 fJ) coincide with LMA sources emitting moderate to high power (greater than 20 dBW). This observation suggests a correlation between the power emissions from the LMA sources and the optical energy measured by the GLM. However, the events with the maximum GLM-optical

energy do not coincide with the stroke locations inside or outside the RLS. Conversely, there is one stroke located within a minimal GLM-optical energy pixel. Therefore, in this instance, the energy of GLM events does not accurately indicate the CG stroke's locations.

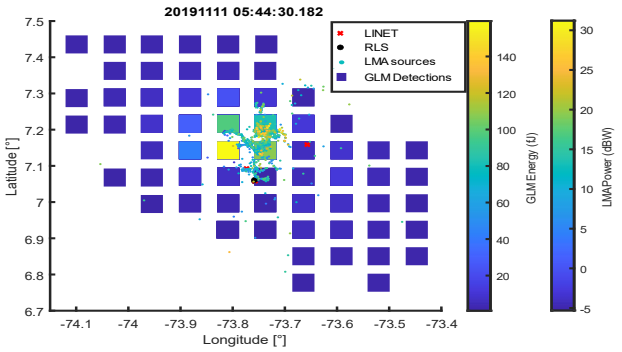

Fig. 5. Top view of CG (×), LMA, and GLM detections for a flash in a RLS on November 11, 2019, at 05:44:30.182 UTC.

C. *Fast downward leaders to RLSs*

Now we investigate the flashes initiating with a downward negative leader striking the RLS tower. We found a 54% of the LMA-flashes in RLSs consist of fast downward leaders without significant horizontal propagation. Figure 6 depicts a case of the group of flashes. Panel A shows a LMA-flash where two CG strokes are occurred at the RLS. The flash starts around 4.7 km (black point) with a fast negative downward leader, resulting in an initial CG stroke of -7 kA. Three subsequent CG strokes with -28.9 kA, -30.3 kA, and -35.4 kA peak currents were registered, the latter occurring on the RLS. These CG strokes are associated with leaders exhibiting a purely downward propagation without horizontal movement. Shortly after the third CG stroke, an in-cloud leader propagated at 6-4 km altitude and downward quickly triggering a second CG stroke in the RLS measuring -30.5 kA. After the last stroke, in-cloud leader activity extended to 5-15 km altitudes for around 350 ms. Panel B has no GLM optical integrated energy during the first stroke.

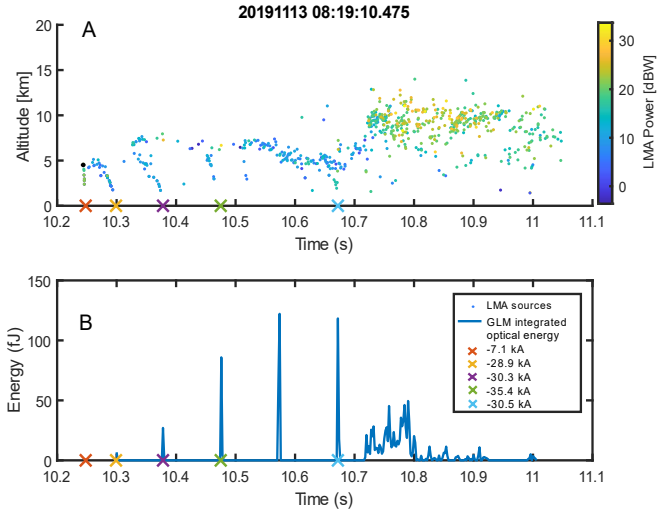

Fig. 6. A) LMA detections altitude vs. time (color-coded by power); B) GLM-integrated optical energy for a flash in a RLS on 13 November 2019 at 08:19:10.475 UTC. Markers (×) indicate the CG strokes.

This absence is attributed to the leader's low starting altitude and its entirely downward propagation. This situation is repeated for leaders exhibiting similar characteristics in other flashes. In the subsequent strokes within the LMA-flash, pulses of integrated energy are observed, with maximum values of 6.733 fJ, 27.01 fJ, 85.85 fJ, and 118.3 fJ. The two highest values correlate with the strokes related to the RLS, coinciding with the highest stroke peak current values. Following the last stroke, continuous report of optical energy was observed in association with the horizontal propagation of the lightning leaders at high altitudes. Significant increases in integrated energy of 45.29 fJ and 49.48 fJ were noted during this process.

The top view of the GLM and LMA detections is shown in Figure 7. The LMA-flash has a maximum horizontal extension of 27.78 km in latitude and 29.58 km in longitude, with power emissions reaching up to 33.7 dBW. The GLM-flash recorded events with optical energy of up to 24.04 fJ, which is significantly lower than the maximum observed in the previous GLM-flash probably due to the in-cloud leaders' altitude and type of propagation. In this case, the CG detections and the RLS location are distant from the GLM's maximum optical energy pixels. This discrepancy is likely because fast negative downward leaders, which initiate and propagate at altitudes below 5 km, do not generate detectable optical signals in the GLM, as is observed in panel B of Figure 6 during the first two strokes. The maximum energy pixels are more closely associated with the horizontal propagation of the leaders at high altitudes, beginning at 10.7 s.

According to the total LMA flashes analyzed, 38% of LMA-flashes record the first stroke at a RLS. Additionally, 40% of LMA-flashes in RLSs involve multiple strokes striking the RLS structure. Notably, in 76% of cases, the stroke with the highest current is recorded at a RLS.

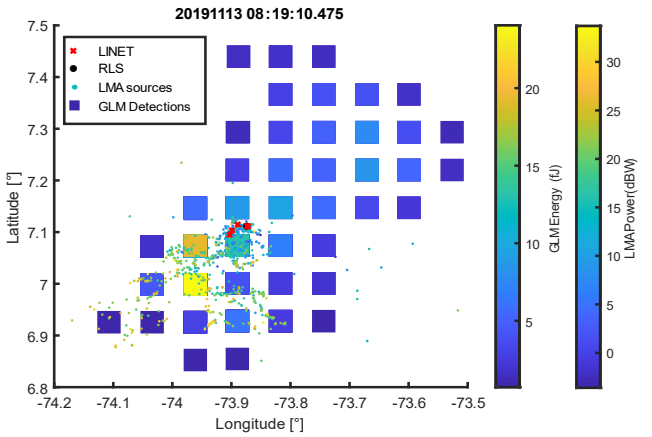

Fig. 7. Top view of CG (×), LMA sources, and GLM pixels for the flash in a RLS on 13 November 2019 at 08:19:10.475 UTC.

D. *Identification of continuing currents*

We found that 16% (8 out of 50) of the flashes in RLS exhibit continuing current. One of these cases is illustrated in Figure 8. According to panel A, the LMA-flash begins with a negative downward leader at 4.9 km altitude propagating for 30 ms and triggering a -65.1 kA CG stroke. Another positive leader extends to altitudes greater than 5 km for 1.4 seconds. During

its propagation it initiates another negative downward leader, resulting in three subsequent strokes of -27 kA, -21.7 kA, and -6.8 kA, respectively. Additionally, 820 ms later, LINET detects a +CG stroke of 11 kA caused by the positive leader mentioned earlier. LMA maps a negative leader from this last stroke, which propagates to heights greater than 10 km. Panel B presents the GLM integrated optical energy during the LMA-flash. It is observed that during the first stroke, no GLM detections were recorded due to the low altitude at which the downward leader began. During the three subsequent negative strokes, the optical energy shows three pulses that correspond to the CG strokes. Following the last +CG stroke, an increase in integrated energy is observed for approximately 80 ms, indicating a long-lasting positive continuous current. The negative leader mapped after the +CG stroke is related to this continuous current supply, propagating to altitudes greater than 10 km, where the upper positive charge region is located.

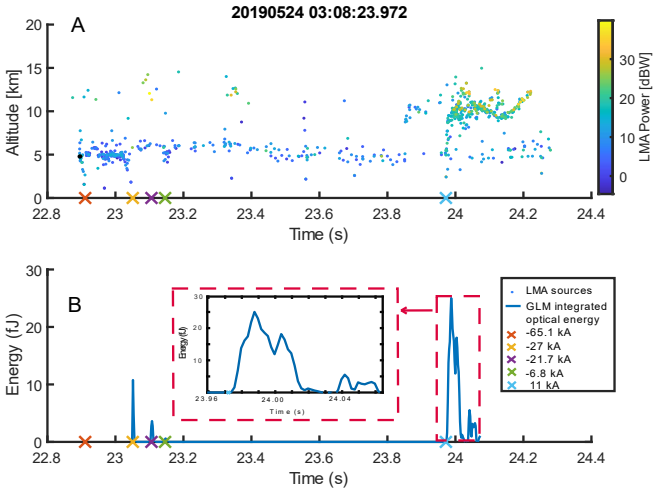

Fig. 8. A) LMA detections altitude vs. time (color-coded by power); B) GLM-integrated optical energy for a flash in a RLS on 24 May 2019 at 03:08:23.972 UTC. Markers (×) indicate the CG strokes.

According to Figure 9, the LMA-flash has a maximum horizontal extension of 19.98 km in latitude and 23.66 km in longitude, with power emissions of up to 40 dBW. The GLM-flash presents events with a maximum energy of 10.68 fJ, occurring far from the location of the strokes and the RLS. These recorded GLM events are closely related to the VHF high-power sources by the LMA. The temporal development of the LMA-flash indicates that these sources correspond to a negative leader providing the continuous current after the +CG stroke.

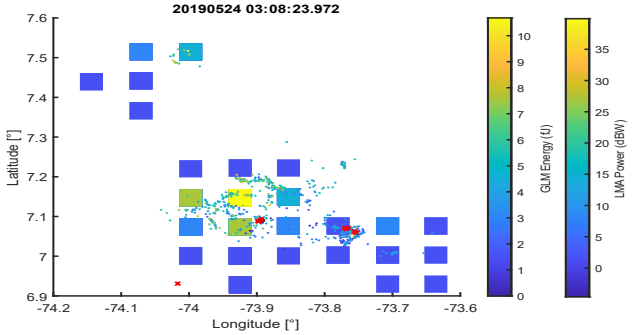

Fig. 9. Top view of CG (×), LMA, and GLM detections for a flash in a RLS on 24 May 2019 at 03:08:23.972 UTC.

E. Stroke peak current and optical energy analysis

GLM-integrated optical energy typically presents pulses associated with the occurrence of CG strokes (e.g. Figure 6 B). In this section we explore if there is any relation between the amplitude of the optical pulses and the stroke peak currents.

Figure 10 plots the cumulative (left axis) and absolute (right axis) frequency histogram of the GLM-integrated optical energy associated with peak currents of CG strokes at RLS and in other locations (OP). For the range between 40 fJ to 160 fJ the largest differences in the cumulative frequency between RLS and other sites (OP) is found. This difference reaches a maximum of 21.51% in the interval between 80 and 90 fJ. Beyond this point, the cumulative frequencies for both groups begin to rise linearly, although the growth for RLS is more pronounced. Regarding median values of the optical energy for the RLS and other locations, the other locations show a median of approximately 25 fJ, while RLS has a higher median of around 35 fJ. Additionally, in the interval with the largest cumulative difference, only 13.56% of strokes at other locations are associated with energies greater than 90 fJ. In contrast, at RLS is 2.6 times higher, reaching 35.07%. Furthermore, 10% of strokes exceed 140 fJ at other locations, while the 90th percentile for RLS rises to 200 fJ, indicating that the strokes associated with RLS are generally more optically energetic for the GLM.

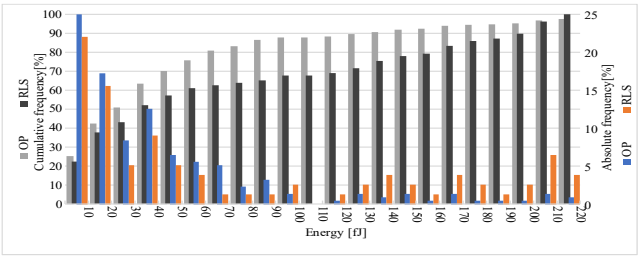

Fig. 10. Histograms of cumulative and relative frequencies of GLM integrated optical energy for strokes in other locations (OP) and at RLS.

This trend is further supported by the histogram of absolute frequencies, which clearly shows that strokes with energies below 90 fJ are more common in other locations, while those above this threshold are more frequent at RLS. For example, 6.49% of strokes at RLS have associated energies between 200 and 210 fJ, whereas only 1.40% of strokes in other areas reach this level.

Now we analyze the peak currents of the CG return strokes in this study. Figure 11 presents the cumulative (left axis) and absolute (right axis) frequency histograms of the peak currents for strokes occurred at RLS and in other places (OP). A significant difference is observed between the accumulated frequencies for currents less than 30 kA, with a maximum difference of 19.62% between 20 and 30 kA. The above suggests a greater occurrence of strokes with lower current values in locations other than RLS. Furthermore, the median current of strokes at other locations falls between 10 and 20 kA, while at RLS, it ranges from 20 to 30 kA. Additionally, 10% of strokes in other places have currents exceeding 30 kA, whereas in RLS, this amount rises to 80 kA. The association of higher currents with RLS is also evident in the absolute frequency histogram, which shows that strokes with currents less than 30 kA are more common in other locations. In contrast, those with

currents above this threshold are more frequent at RLS. Notably, for current values exceeding 100 kA, there is a significant percentage difference between strokes at RLS and those in other locations.

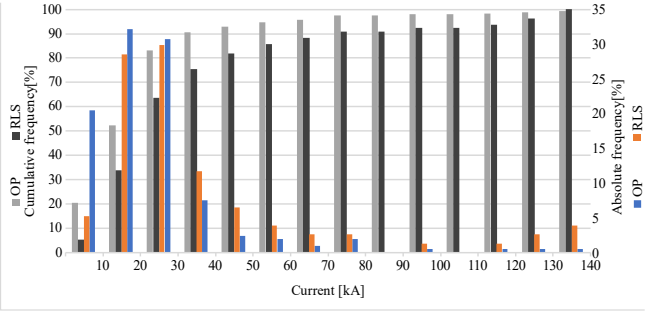

Fig. 11. Histograms of cumulative and relative frequencies of CG return stroke peak current in other locations (OP) and at RLS.

Figure 12 presents a scatter diagram of GLM-integrated optical energy vs current for all RLS strokes classified according to their polarity. It is observed that for -CG strokes, there is no clear pattern or relationship, while for +CG, there is an approximately linear dependence between these two magnitudes.

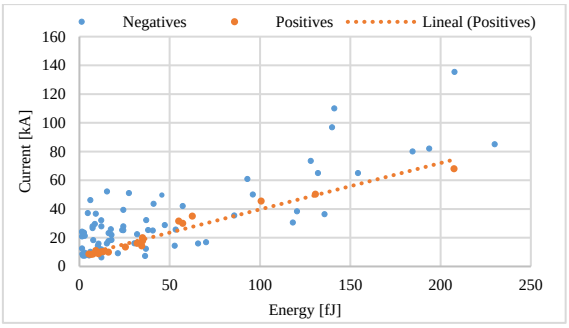

Fig. 12. Scatter diagram of energy vs current for all strokes in RLS classified according to their polarity.

It was also obtained that in 48% of the RLS flashes, the maximum optical energy value corresponds to the stroke in the RLS and, that the strokes not detected by GLM are associated with low stroke peak currents. Likewise, all flashes with strokes in RLS were detected by GLM.

IV. Discussion

Power transmission towers (PTTs) showing a monotonically decreasing average ground strike point density (NSG) are excluded from being classified as RLSs, which is because, from their location up to distances of up to 1 km or more, N_{SG} behaves like in any other location without a PTT. Consequently, these towers do not create lightning recurrence points. This behavior occurs because as one moves away from the PTT, the surrounding area increases quadratically with the radius, and therefore, given a distribution of strokes in the area, NSG will decrease approximately quadratically for all values of radius when the PTT does not correspond to a RLS. Unlike PTTs classified RLS, the presence of a PTT not designated as a RLS does not influence the number of lightning strikes in its vicinity. The above is explained by the fact that near a non-RLS power transmission tower, there is no evidence of a maximum N_{SG} and a subsequent decline as one moves away.

According to the processed LMA-flashes, there were no recorded CG strokes caused by upward flashes from the electric power system tower. Consequently, the lightning-tall tower interaction was entirely triggered by downward-stepped leaders from the thunderstorm charge structure. This phenomenon can be attributed to the fact that in tropical zones, the electrical charge regions during thunderstorms are significantly higher than those in temperate zones [29], [43]. The RLS strokes associated with entirely downward leaders lacking extensive horizontal propagation exhibit the high peak currents. In fact, in 76% of the RLS flashes, the stroke with the highest current is recorded in the RLS, with an average of 42.27 kA. This correlation between high stroke peak currents and RLS is also reflected in the histogram of accumulated and absolute frequencies for stroke currents in RLS compared to other locations. These findings are consistent with studies such as [14], [44], which establish that lightning flashes in tall structures are associated with negative downward flashes with peak currents above the median. This phenomenon can be explained by the striking distance increasing with peak current during the attachment process. As a result, a tall structure is more likely to intercept a downward leader with high charge density at greater distances [15], [45]. Similarly, in [44], it was found that tall strike towers can enhance the electromagnetic field peaks produced by lightning strokes, as this field is determined mainly by the tower itself rather than the lightning channel; the above results in higher current strokes at the tower compared to other locations. However, as in [10] the high peak currents at RLS are not attributed to this effect because this cannot occur in RLS related to orography and not to structures. Moreover, in [46], they found that for cumulative probabilities greater than 76.53%, the difference in stroke currents in RLS and random sites grows exponentially, suggesting that high-peak currents are much more related to RLS. Lightning flashes with entirely downward leaders towards the RLS, typically beginning at altitudes between 3.5 and 6.8 km. According to [43], this altitude corresponds to the lower positive charge region in the thunderstorms analyzed in the study zone. This lower positive charge region may increase the CG flash rates to RLS. This observation is consistent with findings from references [29] and [47], which indicate that the classical tripolar structure is associated with the highest CG flash rates.

Based on the GLM-flashes studied, the maximum GLM-optical energy recorded per pixel is not correlated with the CG stroke's occurrence. However, pulses in the GLM-integrated optical energy, similar to those presented in Figure 6 for four of the five flash strokes, correlate with those. Our analysis showed that in 86% of the flashes, the strokes are not located on the highest energy pixels but instead surrounding them, as demonstrated by [48]. In contrast, 74.13% (235 out of 317) of the optical energy pulses coincide with CG strokes, whether on or off an RLS. These pulses were also reported by [21] during the strokes of a flash over the Morro de Cachimbo tower in Brazil and are indicative of the efficiency of GLM in detecting CG strokes. We found that pulses in the GLM-integrated optical energy were detected in 88 % of strokes in RLS and 79.35% of strokes in other locations. Overall, 82.25% (227 out of 276) of

strokes were identified by GLM, which is comparable to the results found in [49], where detection efficiencies of 86.5% were reported for CG strokes using energy data from GLM groups specifically designed to detect CG strokes [34], [49]. Additionally, a detection efficiency of 89.47% was observed for +CG strokes and 81.32% for -CG strokes. This finding aligns with [50], which reported slightly higher efficiencies that maintained a +CG/-CG proportion equal to the identified in this study. GLM predominantly detects +CG strokes since it initiates in the thunderstorm's mid-level negative region, situated above the lower positive region where -CG strokes begin [29], [43]. The presence of these lower positive charge regions is correlated with the occurrence of CG strokes [47].

We identified four factors influencing the optical energy detected by the GLM. The first is the in-cloud leader's propagation altitude. We observed that flashes, where the in-cloud leaders reached altitudes greater than 10 km, were correlated with maximum optical energy events detected by the GLM. These leaders are identified as negative in-cloud leaders that propagate in the upper positive charge regions, consistent with the electrical charge structures of the storms studied in the area [29], [43]. The second factor relates to the in-cloud leader horizontal extension and the flash duration. We found that a broad horizontal in-cloud leader development in a flash, which translates into a longer duration flash, is correlated with greater optical detections. This finding aligns with previous research such as [49], which reported average efficiencies of 77.8% for flashes extending from 15 to 25 km horizontally. In contrast, the third factor, is related to fast downward negative leaders initiating at heights lower than 5 km producing CG strokes that are not widely detected by the GLM, mainly when they correspond to the initiation of the flash. This observation is supported by [21] and [51] findings. Evidence of this is shown in our work, where 56% of flashes did not have their first stroke detected by GLM. These undetected strokes are mainly caused by downward negative leaders starting at lower altitudes in the cloud and propagating downwards without simultaneous significant in-cloud vertical and horizontal expansion. These negative downward initiate in the boundary of the lower dipole region [52], typically located at heights between 4 and 7 km in the study area [43], making them challenging to detect by GLM. The difficulty in detection of optical emissions from first CG strokes can be explained by the attenuation of the optical emissions due to the large optical depth of the portion of the cloud between the altitude of the flash initiation (4-7 km) and the cloud top typically at 15-18 km [29] in the region of this study. The final factor influencing the energy detected by GLM is the power emitted by the leaders. Leaders with higher emitted VHF power result in proportional optical detections [53]. Fast negative leaders are not associated with high VHF power emissions and this could explain the poor detection from GLM of CG strokes caused by these leaders.

Regarding the relationship between current and integrated optical energy, it is evident that at night, lightning strikes with lower currents are detected much more effectively by the GLM. This improved detection efficiency at night is supported by [49], which reports detection efficiencies of 98.3% at night compared to 84.3% in the day.

V. Conclusions

The findings of this study are summarized as follows:

-The lightning-tall tower interaction was due to downward leaders from the thunderstorm charge regions, with no upward flashes from the structure.
- The highest magnitude of the peak currents of the CG strokes to RLS were produced by fast negative downward leaders initiating at low cloud altitudes without significant simultaneous in-cloud extension of the upper leader channel end.
-Thunderstorms' lower positive charge regions may contribute to increased lightning activity at RLS.
-Pulses in the GLM-integrated optical energy can be associated with CG strokes, allowing to estimating GLM efficiency in detecting CG strokes.
-Four key factors influence the detection of CG flashes by the GLM: the in-cloud leader's propagation altitude, the horizontal extension and duration of the flash, the initiation altitude of the downward leaders producing CG strokes, and the VHF power emitted by the leaders.
-Strokes undetected by GLM are typically related to low peak current strokes and to strokes with their downward leader initiation at low cloud altitudes without precedent or simultaneous in-cloud leader activity.
- GLM detection of +CG strokes is more effective than -CG strokes mainly because of the leader's starting height.
-For positive strokes, there is a nearly linear dependence between the GLM-integrated optical energy and the current. For negative strokes, this dependence is more dispersed.

VI. References

[1] Y. Baba, “Review of recent researches related to lightning to tall structures,” 2010. doi: 10.1541/ieejpes.130.769.

[2] M. A. Uman, *The art and science of lightning protection*. 2008. doi: 10.1017/CBO9780511585890.

[3] A. J. Eriksson, “LIGHTNING AND TALL STRUCTURES.,” *Trans S Afr Inst Electr Eng*, vol. 69, no. pt 8, 1978, doi: 10.1049/piee.1978.0084.

[4] A. J. Eriksson, “The incidence of lightning strikes to power lines,” *IEEE Transactions on Power Delivery*, vol. 2, no. 3, 1987, doi: 10.1109/TPWRD.1987.4308191.

[5] N. Watanabe, A. Nag, G. Diendorfer, H. Pichler, W. Schulz, and H. K. Rassoul, “Characterization of the initial stage in upward lightning at the Gaisberg Tower: 1. Current pulses,” *Electric Power Systems Research*, vol. 213, 2022, doi: 10.1016/j.epsr.2022.108626.

[6] F. Rachidi and M. Rubinstein, “Säntis lightning research facility: a summary of the first ten years and future outlook,” *Elektrotechnik und Informationstechnik*, vol. 139, no. 3, 2022, doi: 10.1007/s00502-022-01031-2.

[7] H. Zhou, N. Theethayi, G. Diendorfer, R. Thottappillil, and V. A. Rakov, “On estimation of the effective height of towers on mountaintops in lightning incidence studies,” *J Electrostat*, vol. 68, no. 5, 2010, doi: 10.1016/j.elstat.2010.05.014.

[8] J. Montanyà *et al.*, “Global distribution of winter lightning: A threat to wind turbines and aircraft,” *Natural Hazards and Earth System Sciences*, 2016, doi: 10.5194/nhess-16-1465-2016.

[9] J. Herrera, C. Younes, and L. Porras, “Cloud-to-ground lightning activity in Colombia: A 14-year study using lightning location system data,” *Atmos Res*, 2018, doi: 10.1016/j.atmosres.2017.12.009.

[10] G. Sola, J. A. López, J. Montanyà, N. Pineda, and E. R. Williams, “Recurrent Lightning Spots: Where Lightning Strikes More Than Twice,” *Journal of Geophysical Research: Atmospheres*, vol. 129, no. 5, Mar. 2024, doi: 10.1029/2023JD040098.

[11] P. Chowdhuri *et al.*, "Parameters of lightning strokes: A review," 2005. doi: 10.1109/TPWRD.2004.835039.

[12] V. A. Rakov *et al.*, "Lightning Parameters for Engineering Applications," in *2010 Asia-Pacific International Symposium on Electromagnetic Compatibility*, 2013.

[13] G. Diendorfer, H. Pichler, and M. Mair, "Some parameters of negative upward-initiated lightning to the gaisberg tower (2000-2007)," *IEEE Trans Electromagn Compat*, vol. 51, no. 3 PART 1, 2009, doi: 10.1109/TEMC.2009.2021616.

[14] S. Visacro, A. Soares, M. A. O. Schroeder, L. C. L. Cherchiglia, and V. J. de Sousa, "Statistical analysis of lightning current parameters: Measurements at Morro do Cachimbo station," *Journal of Geophysical Research: Atmospheres*, 2004, doi: 10.1029/2003jd003662.

[15] M. D. Tran and V. A. Rakov, "When does the lightning attachment process actually begin?," *J Geophys Res*, vol. 120, no. 14, 2015, doi: 10.1002/2015JD023155.

[16] J. Montanyà, O. van der Velde, and E. R. Williams, "Lightning discharges produced by wind turbines," *J Geophys Res*, 2014, doi: 10.1002/2013JD020225.

[17] C. Schumann *et al.*, "On the Triggering Mechanisms of Upward Lightning," *Sci Rep*, vol. 9, no. 1, 2019, doi: 10.1038/s41598-019-46122-x.

[18] N. Pineda, J. Montanyà, A. Salvador, O. A. van der Velde, and J. A. López, "Thunderstorm characteristics favouring downward and upward lightning to wind turbines," *Atmos Res*, 2018, doi: 10.1016/j.atmosres.2018.07.012.

[19] J. Montanyà, O. Van Der Velde, A. Domingo-Dalmau, N. Pineda, O. Argemí, and A. Salvador, "Lightning mapping observations of downward lightning flashes to wind turbines," in *2016 33rd International Conference on Lightning Protection, ICLP 2016*, 2016. doi: 10.1109/ICLP.2016.7791449.

[20] J. Figueras I Ventura *et al.*, "Polarimetric radar characteristics of lightning initiation and propagating channels," *Atmos Meas Tech*, vol. 12, no. 5, 2019, doi: 10.5194/amt-12-2881-2019.

[21] J. Montanyà *et al.*, "Potential use of space-based lightning detection in electric power systems," *Electric Power Systems Research*, vol. 213, 2022, doi: 10.1016/j.epsr.2022.108730.

[22] A. Mostajabi *et al.*, "LMA observation of upward flashes at Säntis Tower: Preliminary results," in *2018 IEEE International Symposium on Electromagnetic Compatibility and 2018 IEEE Asia-Pacific Symposium on Electromagnetic Compatibility, EMC/APEMC 2018*, 2018. doi: 10.1109/ISEMC.2018.8393808.

[23] N. Pineda *et al.*, "Meteorological Aspects of Self-Initiated Upward Lightning at the Säntis Tower (Switzerland)," *Journal of Geophysical Research: Atmospheres*, vol. 124, no. 24, 2019, doi: 10.1029/2019JD030834.

[24] S. Visacro, C. R. Mesquita, A. De Conti, and F. H. Silveira, "Updated statistics of lightning currents measured at Morro do Cachimbo Station," *Atmos Res*, 2012, doi: 10.1016/j.atmosres.2011.07.010.

[25] H. D. Betz *et al.*, "LINET-An international lightning detection network in Europe," *Atmos Res*, 2009, doi: 10.1016/j.atmosres.2008.06.012.

[26] D. Aranguren, J. López, J. Inampués, H. Torres, and H. Betz, "Cloud-to-ground lightning activity in Colombia and the influence of topography," *J Atmos Sol Terr Phys*, 2017, doi: 10.1016/j.jastp.2016.08.010.

[27] K. L. Cummins and M. J. Murphy, "An overview of lightning locating systems: History, techniques, and data uses, with an in-depth look at the U.S. NLDN," 2009. doi: 10.1109/TEMC.2009.2023450.

[28] K. L. Cummins, M. J. Murphy, E. A. Bardo, W. L. Hiscox, R. B. Pyle, and A. E. Pifer, "A combined TOA/MDF technology upgrade of the US National Lightning Detection Network," *Journal of Geophysical Research Atmospheres*, 1998, doi: 10.1029/98JD00153.

[29] J. A. López *et al.*, "Charge Structure of Two Tropical Thunderstorms in Colombia," *Journal of Geophysical Research: Atmospheres*, 2019, doi: 10.1029/2018JD029188.

[30] W. Rison, R. J. Thomas, P. R. Krehbiel, T. Hamlin, and J. Harlin, "A GPS-based three-dimensional lightning mapping system: Initial observations in central New Mexico," *Geophys Res Lett*, 1999, doi: 10.1029/1999GL010856.

[31] D. E. Proctor, "VHF radio pictures of cloud flashes," *J Geophys Res Oceans*, vol. 86, no. C5, 1981, doi: 10.1029/jc086ic05p04041.

[32] P. R. Krehbiel, R. J. Thomas, W. Rison, T. Hamlin, J. Harlin, and M. Davis, "GPS-based mapping system reveals lightning inside storms," *Eos (Washington DC)*, 2000, doi: 10.1029/00EO00014.

[33] J. A. López *et al.*, "Initiation of lightning flashes simultaneously observed from space and the ground: Narrow bipolar events," *Atmos Res*, vol. 268, 2022, doi: 10.1016/j.atmosres.2021.105981.

[34] S. J. Goodman, R. Blakeslee, and W. Koshak, "Geostationary lightning mapper for GOES-R.," *Star*, vol. 45, no. 26, 2008.

[35] S. J. Goodman *et al.*, "The GOES-R Geostationary Lightning Mapper (GLM)," *Atmos Res*, vol. 125–126, 2013, doi: 10.1016/j.atmosres.2013.01.006.

[36] D. M. Mach, H. J. Christian, R. J. Blakeslee, D. J. Boccippio, S. J. Goodman, and W. L. Boeck, "Performance assessment of the Optical Transient Detector and Lightning Imaging Sensor," *Journal of Geophysical Research Atmospheres*, vol. 112, no. 9, 2007, doi: 10.1029/2006JD007787.

[37] D. M. Mach, "Geostationary Lightning Mapper Clustering Algorithm Stability," *Journal of Geophysical Research: Atmospheres*, vol. 125, no. 5, 2020, doi: 10.1029/2019JD031900.

[38] Keraunos S.A.S, "Red Colombiana de detección total de rayos - LINET," 2015.

[39] R. Said, E. Grimit, and M. Murphy, "A Multiyear CONUS-Wide Analysis of Lightning Strikes to Wind Turbines," *Wind Energy*, vol. 28, no. 3, Mar. 2025, doi: 10.1002/we.70000.

[40] O. A. Van Der Velde and J. Montanyà, "Asymmetries in bidirectional leader development of lightning flashes," *Journal of Geophysical Research Atmospheres*, 2013, doi: 10.1002/2013JD020257.

[41] J. A. López, N. Pineda, J. Montanyà, O. van der Velde, F. Fabró, and D. Romero, "Spatio-temporal dimension of lightning flashes based on three-dimensional Lightning Mapping Array," *Atmos Res*, 2017, doi: 10.1016/j.atmosres.2017.06.030.

[42] J. Roncancio, J. Montanyà, J. López, M. Urbani, and O. van der Velde, "Investigation of GLM detections of negative continuing currents observed by high-speed video and narrow-band 777 nm photometer," *Electric Power Systems Research*, vol. 239, p. 111250, Feb. 2025, doi: 10.1016/j.epsr.2024.111250.

[43] B. S. Ardila Murillo, E. A. Soto Ríos, D. Argüello Barbosa, H. Tello Rodríguez, J. López Trujillo, and J. Montanyà, "Análisis de estructuras de carga de dos tormentas eléctricas registradas por la red Lightning Mapping Array en el Magdalena Medio colombiano," *Ingeniería*, vol. 27, no. 2, 2022, doi: 10.14483/23448393.17925.

[44] D. Pavanello *et al.*, "On return stroke currents and remote electromagnetic fields associated with lightning strikes to tall structures: 1. Computational models," *Journal of Geophysical Research Atmospheres*, vol. 112, no. 13, 2007, doi: 10.1029/2006JD007958.

[45] S. Visacro, M. Guimaraes, and M. H. Murta Vale, "Striking Distance Determined From High-Speed Videos and Measured Currents in Negative Cloud-to-Ground Lightning," *Journal of Geophysical Research: Atmospheres*, vol. 122, no. 24, 2017, doi: 10.1002/2017JD027354.

[46] S. Ardila, G. Solà, J. López, and J. Montanyà, "Tall structures as Recurrent Lightning Spots in the inner tropics," in *International Conference on Lightning Protection ICLP* , Dresde, Germany, 2024.

[47] A. Salvador, N. Pineda, J. Montanyà, J. A. López, and G. Solà, "Thunderstorm charge structures favouring cloud-to-ground lightning," *Atmos Res*, 2021, doi: 10.1016/j.atmosres.2021.105577.

[48] O. A. van der Velde *et al.*, "Comparison of High-Speed Optical Observations of a Lightning Flash From Space and the Ground," *Earth and Space Science*, vol. 7, no. 10, 2020, doi: 10.1029/2020EA001249.

[49] D. Zhang and K. L. Cummins, "Time Evolution of Satellite-Based Optical Properties in Lightning Flashes, and its Impact on GLM Flash Detection," *Journal of Geophysical Research: Atmospheres*, vol. 125, no. 6, 2020, doi: 10.1029/2019JD032024.

[50] A. F. R. Leal and V. A. Rakov, "Processes in negative and positive CG lightning flashes detected from space by GLM," *Electric Power Systems Research*, vol. 229, p. 110183, Apr. 2024, doi: 10.1016/j.epsr.2024.110183.

[51] J. Montanyà *et al.*, "A Simultaneous Observation of Lightning by ASIM, Colombia-Lightning Mapping Array, GLM, and ISS-LIS," *Journal of Geophysical Research: Atmospheres*, vol. 126, no. 6, 2021, doi: 10.1029/2020JD033735.

[52] P. R. Krehbiel *et al.*, "Upward electrical discharges from thunderstorms," *Nat Geosci*, vol. 1, no. 4, pp. 233–237, Apr. 2008, doi: 10.1038/ngeo162.

[53] J. A. Roncancio, J. Montanyà, J. A. López, M. Urbani, O. A. van der Velde, and M. Arcanjo, "Ground-Based Observations of 337 nm and 777 nm Optical Emissions Produced by Lightning," *Journal of Geophysical Research: Atmospheres*, vol. 129, no. 10, May 2024, doi: 10.1029/2024JD040836.